The effect of fluorine doping and temperature on the field emission from diamond-like carbon films

2007 J. Phys.: Condens. Matter 19 346233

(http://iopscience.iop.org/0953-8984/19/34/346233)

IOP PUBLISHING JOURNAL OF PHYSICS: CONDENSED MATTER

J. Phys.: Condens. Matter **19** (2007) 346233 (15pp) doi:10.1088/0953-8984/19/34/346233

The effect of fluorine doping and temperature on the field emission from diamond-like carbon films

Sk F Ahmed[1], **M K Mitra**[2] **and K K Chattopadhyay**[1,2,3]

[1] Thin Film and Nanoscience Laboratory, Department of Physics, Jadavpur University, Kolkata 700 032, India
[2] Nanoscience and Technology Center, Jadavpur University, Kolkata 700 032, India

E-mail: kalyan_chattopadhyay@yahoo.com

Received 14 May 2007, in final form 10 July 2007
Published 31 July 2007
Online at stacks.iop.org/JPhysCM/19/346233

Abstract

The effects of temperature and fluorine concentration on the field emission properties of diamond-like carbon (DLC) films were studied in detail. The atomic percentage of fluorine in the films was varied from 0 to 15.3 at.% as measured from energy-dispersive analysis of x-rays. The chemical bindings were investigated by x-ray photoelectron spectroscopic studies. Surface morphologies of the F:DLC films were studied by an atomic force microscope, which indicated an increase of surface roughness with fluorine doping percentage. The threshold field was found to decrease from 8.5 to 2.9 V μm^{-1} with a variation of fluorine atomic percentage in the films from 0 to 15.3. The emission properties for a 15.3 at.% F-doped DLC film have been studied for different anode–sample spacing and for different ambient temperature. The temperature-dependent field emission studies of the F:DLC films showed that the threshold field was in the range 4.2–2.2 V μm^{-1} for variation of ambient temperature from 25 to 300 °C. The threshold field and work function have been calculated, and we have tried to explain the emission mechanism therefrom. It was found that the threshold field and effective emission barrier were reduced by F doping compared with undoped DLC.

1. Introduction

Amorphous diamond-like hydrogenated carbon (a-C:H) films have been produced and systematically studied for several decades. Nowadays there is a good knowledge of the behaviour, characteristics and structure of these films in relation to the deposition process parameters, as reported by many authors. DLC films have also found applications in tribology [1, 2], mechanics [1–3], electronics [1, 2], and biomedical [1, 4] fields. The properties of DLC may be modified by the incorporation of dopants, such as silicon, fluorine, nitrogen,

[3] Author to whom any correspondence should be addressed.

oxygen, and various metals. Many applications have been developed for these coatings and their modified counterparts. Among them, great interest has been focused on the fluorine-modified DLC (a-C:F) films, because fluorine doped into the DLC matrix greatly reduces the surface free energy, changes the refractive index and optical band gap, reduces the dielectric constant, etc [5–8]. During the last decade, the advent of low macroscopic field emission from carbon-based films, such as diamond, diamond-like carbon (DLC), amorphous carbon (a-C), carbon nanotube/nanofibres, etc [9, 10] made them the candidate materials for field emission displays. The field emission properties of DLC films are mainly dependent on the variation of chemical bonding structure other than surface roughness, and the doping of material such as boron, phosphorous, nitrogen and silicon into the DLC films [11–13]. One of the most effective ways to change the physiochemical properties of carbon-based material is fluorination. Lai *et al* [14] studied the electron field emission properties of a-C:F nanostructures. They showed that for a-C:F nanoporous films, the turn-on field (1.8 V μm^{-1}) is lower than for other types of a-C:F nanostructures, and the field enhancement factor of an a-C:F nanostructure is greater than that of nonaligned multiwalled nanotubes. A literature survey indicates that there is no published report of the detailed effect of temperature and F concentration on the field emission properties of F:DLC films. The study of field emission from materials at higher temperature is interesting for many reasons. Apart from display applications, the field emission can be applied for other applications: for example, for direct thermal to electrical energy conversion, design of nanothermometer [15], etc. High emission current density is also required for many applications like in electron microscopes, where field emission at higher temperature may also be utilized. Apart from the technological aspect, studies on the effect of temperature on the field emission property helps in detailed understanding of the emission mechanism in a better way. In this work we report the effect of fluorine doping and ambient temperature on the field emission properties of DLC films. The threshold field and field enhancement factor are calculated.

2. Experimental details

2.1. Synthesis of fluorinated diamond-like carbon films

The plasma enhanced chemical vapour deposition (PECVD) chamber was designed with appropriate stainless steel (SS) vacuum couplings through which different feed-throughs like the vacuum port, pressure gauge, gas mixture inlets, thermocouple, etc could be introduced. The plasma was produced between two parallel plate SS electrodes. The lower disc, upon which the substrate was placed, was grounded. A substrate heating arrangement was made with an appropriate substrate heater placed on the grounded electrode. The upper disc was used as the cathode electrode. When the chamber pressure reached 10^{-6} mbar, C_2H_2 gas was introduced and diamond-like carbon films were deposited at a pressure of 0.15 mbar. The substrates, glass and silicon were cleaned by a standard cleaning procedure before they were placed in the deposition chamber. Deposition was made at 2.0 kV DC supply, and the corresponding current density was 12.5 mA cm^{-2} for 20 min. For fluorine incorporation, hydrofluoric acid (HF) dissolved in methanol solution was used. Ar gas was passed through the solution for bubble formation and then introduced into the chamber with an appropriate needle valve arrangement. The fluorine percentage was varied in the deposited films by varying the concentration of HF in the methanol solution.

2.2. Characterizations

The compositions of the films (F, C) were determined by energy-dispersive x-ray analysis (EDX, Oxford, model-7582). Bonding information and an approximate sp^2/sp^3 ratio in

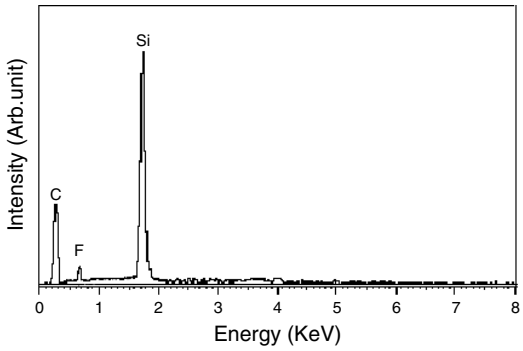

Figure 1. EDX spectrum of an F:DLC film deposited with 13% HF in methanol.

the deposited films were investigated by a Fourier transform infrared spectrophotometer (FTIR, Shimadzu-8400-S). The surface morphology of the films was studied with an atomic force microscope (AFM, NT-MDT, Solver Pro) in contact mode. The carbon and fluorine bonding configuration of the DLC films were determined by x-ray photoelectron spectroscopy (XPS). The analysis was performed on the samples using a Specs (Germany) system with a hemispherical energy analyser. A non-monochromatic Mg Kα x-ray (1253.6 eV) was used as the excitation source, operated at 10 kV and with an anode current 17 mA. The residual pressure of the system was $\sim 10^{-9}$ mbar. The electron field emission properties of the F:DLC films deposited on glass substrates have been studied by our high vacuum ($\sim 10^{-7}$ mbar) field emission set-up [16]. Field emission measurements were carried out by using a diode configuration consisting of a cathode (the film under test) and a stainless steel tip anode mounted in a liquid nitrogen trapped rotary-diffusion vacuum chamber with appropriate chamber baking arrangement. The measurements were performed at a base pressure of $\sim 5 \times 10^{-7}$ mbar and at different temperature, which was controlled with a controller and measured with a thermocouple. The tip–sample distance was continuously adjustable to a few hundred micrometres by a spherometric arrangement with screw-pitch of 10 μm. The anode–sample spacing was set at a particular value by rotating the micrometer screw which served as an anode electrode. Field emission current–voltage measurements were made with the help of an Agilent multimeter (model 3440-1A). The emission characteristics were registered and analysed with the help of a personal computer.

3. Results and discussion

3.1. Compositional analysis

The compositions of the films (F, C) deposited on silicon substrate were determined by energy-dispersive x-ray analysis. Figure 1 shows a typical EDX spectrum of the fluorinated DLC film deposited on silicon substrate. It was seen that the atomic percentage of fluorine in the films was nearly the same as that of the nominal concentration of HF in the methanol solution. The peak of Si appeared due to silicon substrate. Table 1 shows the composition of the films for different HF concentration.

3.2. Fourier-transformed infrared spectra studies

Fourier-transformed infrared (FTIR) absorbance spectra were recorded by taking Si as a reference and subtracting the absorption due to the Si substrate. The FTIR spectrum showed

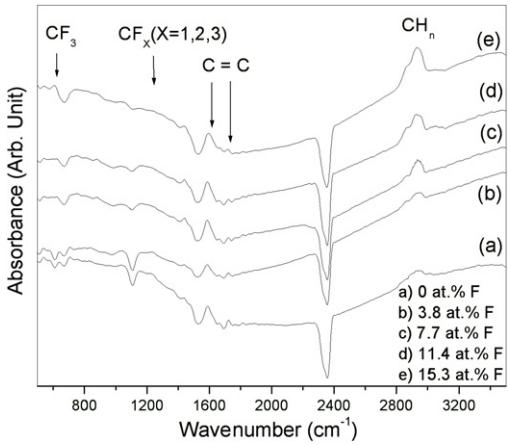

Figure 2. FTIR absorbance spectra of DLC films for different atomic percentage of fluorine.

Table 1. Comparison of threshold field for different atomic percentage of F in the DLC films from EDX measurements.

Sample name	Nominal % of HF in solution	Atomic % F from EDX	Threshold field (V μm^{-1})
F:DLC-3	0	0	8.5
F:DLC-6	4	3.8	6.5
F:DLC-10	8	7.7	5.4
F:DLC-12	13	11.4	4.3
F:DLC-15	17	15.3	2.9

Table 2. Assignment of different C–H vibrational modes of DLC film.

Wavenumbers (cm^{-1})	Vibrational modes
2854	sp^3-CH_2 (symmetric)
2873	sp^3-CH_3
2902	sp^3-CH stretching
2927	sp^3-CH_2 (asymmetric)
2957	sp^3-CH_3 (asymmetric)
2987	sp^3-CH_3
3009	sp^2-CH (symmetric)
3022	sp^2-CH (asymmetric)

different vibrational modes of various bondings. In figure 2, graph (a) shows the FTIR spectrum of the undoped DLC film deposited on Si substrate. The broad peak around 2950 cm^{-1} is assigned to the different C–H$_n$ group stretching modes [17] and the band around 1600 cm^{-1} is due to the C=C stretching mode [17]. Figure 2 graphs (b)–(e) show the FTIR spectra of the fluorine-doped DLC films deposited on Si substrate. Apart from the different C–H vibrational bonds which occur in undoped DLC films, a few new bands appear due to fluorine doping. The absorption peaks at 1450 and 1050 cm^{-1} are associated with C–F, C–F$_2$, and C–F$_3$ stretching modes [18]. It has been found that with the increase of fluorine content in the films, the intensity of the C–H absorption band around 2950 cm^{-1} was increased. Table 2 shows the different vibrational wavenumbers that appeared in the spectra and their assignments to

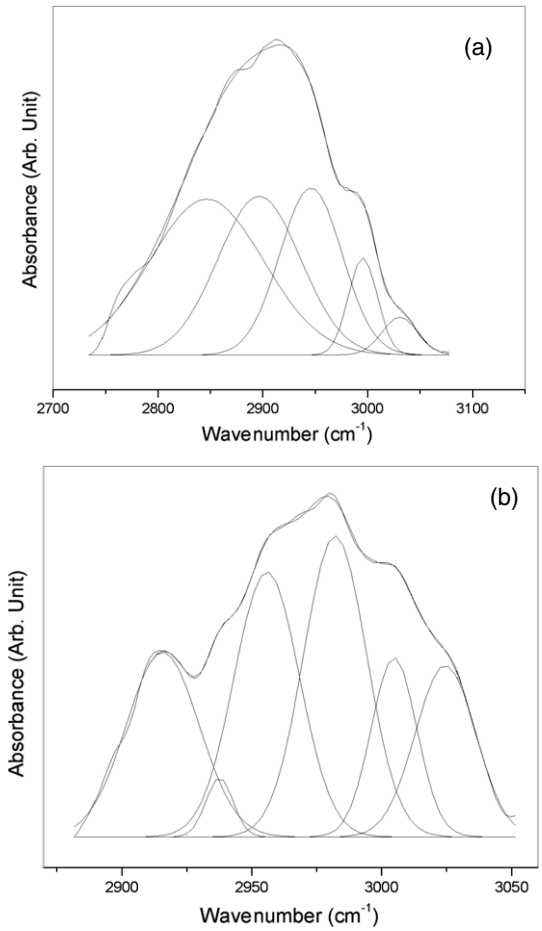

Figure 3. Deconvolution of the C–H band (a) for undoped and (b) for 11.4 at.% F:DLC films.

various C–H bondings. To find the sp^2/sp^3 ratio, the region around the C–H absorption band was deconvoluted into a number of Gaussian peaks by using a computer programme. It has been popular to fit C–H bands with Gaussian peaks to derive sp^2 fractions. As an example, figures 3(a) and (b) show the deconvoluted spectra for the C–H absorption region in the FTIR spectrum of undoped and 15.3 at.% fluorine-doped DLC films (the others are not shown here). Figure 4 shows the variation of sp^2/sp^3 in the films for different atomic percentages of F. It is clear from the figure that the sp^2 content in the films increases with increase of fluorine concentration in the films. A similar type of observation has been reported by other authors [18, 19]. However, it should be mentioned in this connection that the determination of the sp^2/sp^3 ratio in the DLC film from the FTIR spectra is an approximate method because of the possible presence of unbound hydrogen. The Urbach parameter was also calculated from the optical absorption band tails (not shown here) to find out the changes of defect densities with the percentages of F doping. It was observed that the Urbach parameter increased with percentage of F doping in the films, indicating an increase of defects with increasing F percentage. It may be mentioned that the increase of sp^2 fractions and defect density with F doping was also observed by other researchers [20].

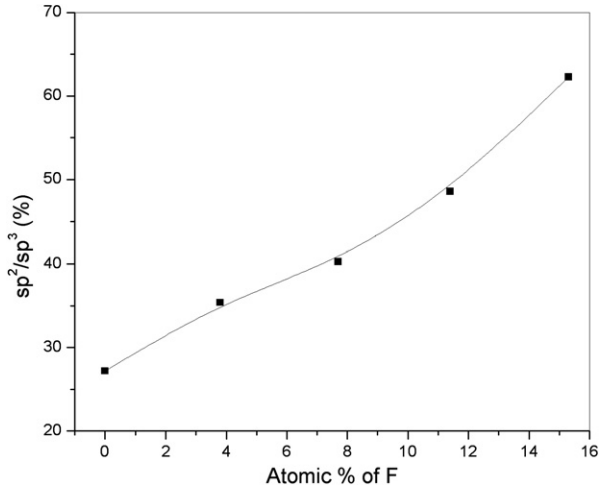

Figure 4. Variation of sp^2/sp^3 ratio with fluorine percentage in the DLC films.

3.3. Structural characterization

AFM imaging provides more detailed information involving the surface morphology and homogeneity of the F:DLC films. Figure 5 shows typical AFM images of (a) undoped (without fluorine) and (b) fluorine-doped (15.3 at.%) DLC films, respectively. The measured surface roughness shows that the surfaces of the F:DLC films are rougher than that of the undoped DLC film. The undoped DLC film generally exhibits a very smooth morphology, with a root mean square (RMS) roughness of 1.1 nm within the surface area of 5 μm $\times$ 5 μm (shown in figure 5(a)). However, the RMS roughness of the F-doped DLC film is approximately 2.5 nm within the same area of 5 μm $\times$ 5 μm (shown in figure 5(b)). The surface roughness increased with increased F percentage in the films. Most likely the increased surface roughness is due to the etching effect of fluorine. The presence of F atoms in the plasma alters the growth condition and it is observed that the percentages of sp^2-bonded carbon increased with increasing F concentration, as discussed in section 3.2. Etching of the growing films by F atoms present in the plasma also takes place. Many other authors also have reported increase of the sp^2/sp^3 ratio and increased surface roughness with F incorporation [18, 19] in DLC films.

3.4. XPS analysis

The XPS survey scan of the fluorinated DLC films clearly shows the contributions from C 1s ($\sim$284 eV), F 1s ($\sim$687 eV) and O 1s ($\sim$532 eV). A typical spectrum of a fluorinated DLC film is shown in figure 6(a). Quantification in XPS was done by CASA-XPS version 2.0 software with Shirley background correction. Figure 6(b) shows the C 1s background-corrected XPS core level spectra of the 15.3 at.% F-doped DLC film. The C 1s peaks obtained in this study are broad. This implies possible contributions from differently bonded carbons to the C 1s peak. Deconvolution of the spectra showed that the broad C 1s peaks are composed of four peaks corresponding respectively to –C–C and –C–CH (284.7 $\pm$ 0.2 eV), –C–CF and –C=O (287.2 $\pm$ 0.1 eV), C–F (289.5 $\pm$ 0.1 eV) and C–F_2 (291.9 $\pm$ 0.2 eV) bonding configurations [21, 22]. However, our XPS spectra do not show any unbound fluorine, as the peak that appeared is chemically shifted, indicating that bonded F was present in the film. The carbon–carbon double bond, C=C, appearing at $\sim$284.7 eV can be assigned to the sp^2 bonding

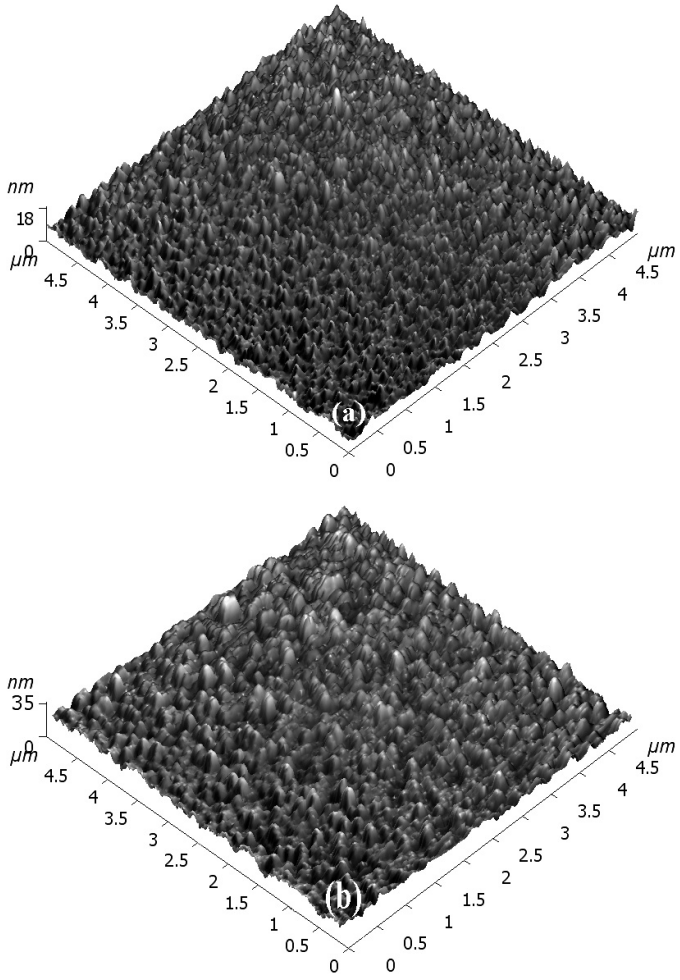

Figure 5. Three-dimensional (3D) AFM images of DLC films: (a) without F and (b) with 15.3 at.% F.

configuration in the films. From the integrated area the amount of oxygen detected in the films was <3%; the oxygen normally comes either from surface contamination due to air exposure or from the use of methanol during deposition. Since XPS is a very surface-sensitive technique, the detection of oxygen suggests various sources of surface contamination. The peaks of Si 2p (∼100 eV) and Si 2s (151 eV) are due to the substrate.

3.5. Field emission studies

Figure 7(a) shows the emission current density (J) versus macroscopic field (E) curves of for F:DLC films for different atomic percentage of fluorine at fixed anode–sample separation (d) of 100 μm. The macroscopic field (E) is calculated from the external voltage applied (V), divided by the anode–sample spacing (d). Theoretically, the emission current I is related to the macroscopic electric field E by

$$I = Aat_{\mathrm{F}}^{-2}\phi^{-1}(\beta E)^2 \exp\left\{\frac{-bv_{\mathrm{F}}\phi^{3/2}}{\beta E}\right\} \tag{1}$$

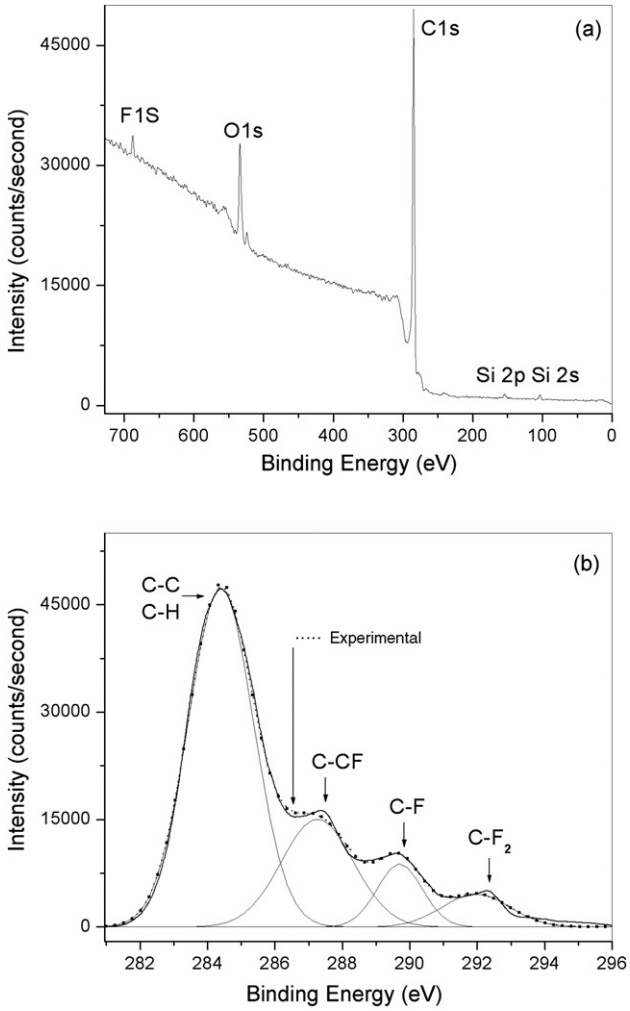

Figure 6. (a) The XPS spectra of the 15.3 at.% F:DLC films deposited on silicon substrate and (b) deconvolution of the XPS spectra in the C 1s peak of the 15.3 at.% F content F:DLC film.

where ϕ is the local work function, β is the field enhancement factor, A is the effective emission area, a is the first Fowler–Nordheim constant ($1.541\,434 \times 10^{-6}$ A eV V^{-2}), b is the second FN constant ($6.830\,890 \times 10^{9}$ eV$^{-3/2}$ V m^{-1}), and v_{F} and t_{F} are the values of the special field emission elliptic functions [23] v and t, evaluated for a barrier height ϕ. The field emission characteristics of the films were analysed using the Fowler–Nordheim (FN) theory. A simplified FN equation for the local current density J (I/A, A cm^{-2}, A = anode–tip area) at some point on the emitting surface may be written as

$$\ln\left\{\frac{J}{E^2}\right\} = \ln\{t_{\mathrm{F}}^{-2} a\phi^{-1}\beta^2\} - \frac{(v_{\mathrm{F}} b\phi^{3/2}\beta^{-1})}{E}. \tag{2}$$

The experimental FN plot is modelled by the tangent to this curve, taken from the experimental data. This tangent can be written in the form [24]

$$\ln\left\{\frac{J}{E^2}\right\} = \ln\{ra\phi^{-1}\beta^2\} - \frac{(sb\phi^{3/2}\beta^{-1})}{E} \tag{3}$$

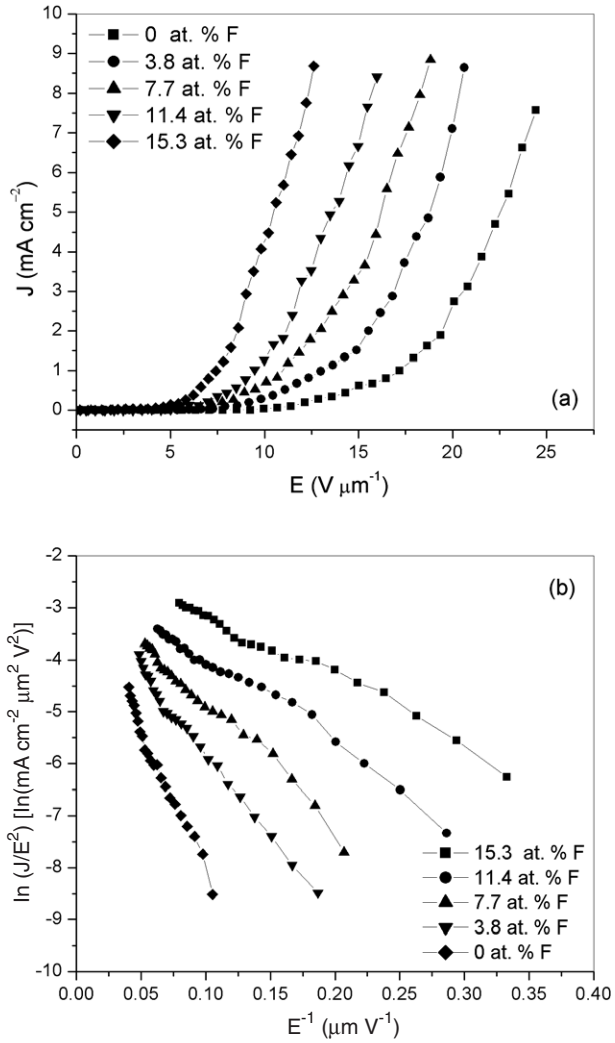

Figure 7. (a) Emission current density (J) versus macroscopic field (E) curves of F:DLC films for different atomic percentage of F. (b) FN plot of F:DLC thin films for different atomic percentage of F.

where r and s are appropriate values of the intercept and slope correction factors, respectively. Typically, s is of the order of unity, but r may be of order 100 or greater. Both r and s are relatively slowly varying functions of $1/E$, so an FN plot (plotted as a function of $1/E$) is expected to be a good straight line. The FN plots of our sample are shown in figure 7(b). It has been observed that all the J–E curves in the present work are satisfactorily fitted with the FN equation (equation (3)). This suggests that the electrons are emitted by a field emission process. The threshold field (E_{th}), which we define as the macroscopic field needed to get an emission current density $J = 10\ \mu\text{A cm}^{-2}$, was in the range 8.5–2.9 V μm^{-1} with a variation of fluorine atomic percentage in the films 0%–15.3%. It has been observed that the threshold field was greatly reduced for the fluorinated DLC films compared to that of the film grown without fluorine. This value is considerably lower than that of nanocrystalline carbon

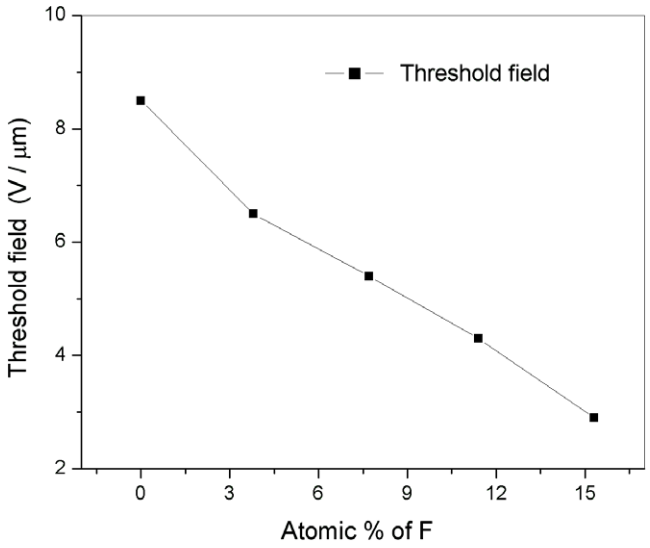

Figure 8. Variation of threshold field with atomic percentage of F in the DLC films.

(6.4 V μm^{-1}) [25], nitrogen-doped DLC (4 V μm^{-1}) [13], sulfur-incorporated nanocrystalline carbon (4 V μm^{-1}) [12] and carbon nanofibre arrays ($\sim$3 V μm^{-1}) reported by Cao *et al* [26]. The values of threshold field for different fluorine atomic percentage in the films is shown in figure 8. The plots of emission current density versus electric field are shown in figure 9(a) and the corresponding FN plots are shown in figure 9(b) for different anode–sample distance. The threshold field was found to vary in the range 2.6–4.3 V μm^{-1} for a variation of anode–sample spacing 80–120 μm, for the 15.3 at.% fluorinated DLC film. In the J–E graph (figure 9(a)), we observed a parallel shift of curves with respect to anode–sample separation (d), i.e., for a particular electric field the current density increases on increasing the anode–sample separation. Zhou *et al* [27] reported a similar type of observation for their β-SiC nanorods. This type of shift observed in our sample is due to the change in the effective emission area of the sample for different anode–sample separation. In our experiment we have used a conical shape anode with tip diameter 1 mm; therefore the lines of force emerging from the edge of the anode tip and terminating at the sample surface are diverging in nature, whereas the lines of force emerging from the flat surface of the tip are parallel in nature. Hence, the effective emission area of the sample increases with increasing d. Au *et al* [28] performed field emission studies of silicon nanowires using a spherical-shaped stainless steel probe with a tip diameter of 1 mm as an anode. They also found a parallel shift in their I–V curve. Okano *et al* [29] reported that their macroscopic current density for diamond films was independent of the anode–sample separation. Their field emission apparatus consisted of a parallel plate arrangement of the anode and sample, separated by spacers. So the electric lines of force between the anode and the sample were parallel in nature; hence the effective emission area remained independent of the anode–sample spacing.

Assuming a plane flat emitter with $\beta = 1$, the emission barriers (ϕ) were calculated from the slopes of the FN plots. The value of ϕ was reduced from 0.040 to 0.015 eV for an optimum F incorporation. But the true barrier must be larger than these values. Such a low work function obtained may be due to an underestimation of the field enhancement factor β. But these values of barriers are unrealistic. Such low barriers are not compatible with field electron emission and are significantly lower than the 2.5–3.5 eV electron affinity found in amorphous

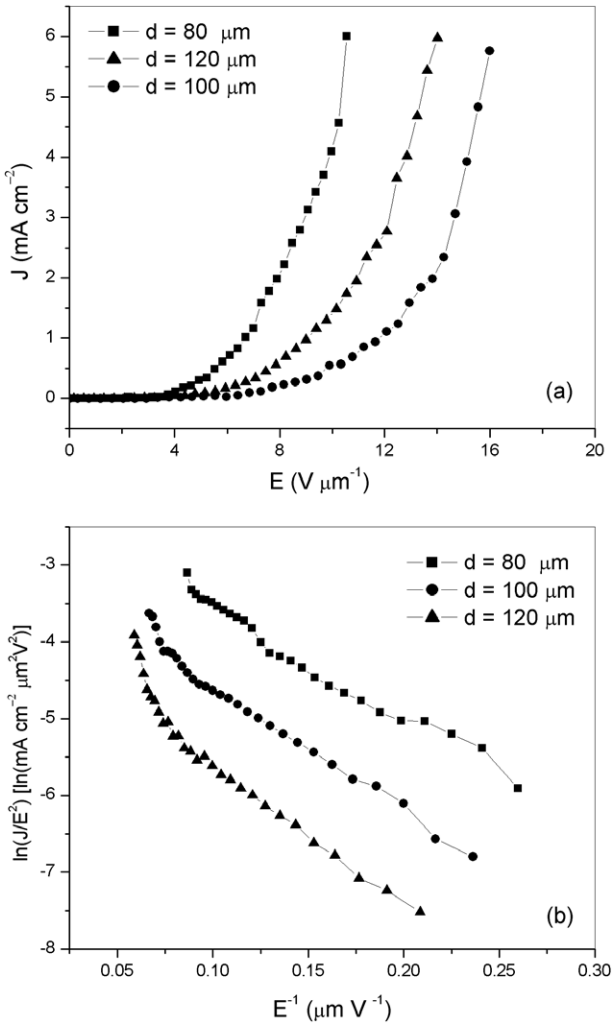

Figure 9. (a) J–E curves for the F:DLC (15.3 at.% F) for different anode–sample separation (d). (b) FN plot of F:DLC (15.3 at.% F) for different anode–sample separation (d).

carbon material [30]. The emission mechanism may involve a strong field enhancement at the front surface. To understand the FN emission process in our F:DLC films, it is necessary to explain the origin of the large enhancement factor required to lower the barrier for easy electron emission. Ilie *et al* [31] and Carey *et al* [32] proposed that the presence of sp^2 clusters within the insulating sp^3 matrix could give rise to field enhancement in amorphous carbon (a-C) films containing large defect densities ($>10^{19}$ cm^{-3}). It was proposed that the presence of such dielectric inhomogeneity [33] is responsible for field enhancement in these films. Since sp^2 clusters will have different dielectric constants, the application of the external field will result in local field enhancements around the clusters and will aid in the emission of electrons. Groning *et al* [34] explained the emission mechanism from DLC films in a way that, like a freestanding conductive tip in the vacuum, sp^2-bonded carbon clusters are assumed to form a conductive channel in an insulating matrix, which leads to local field enhancement and hence to an enhanced electron emission. Since the sp^2 clusters are located at or near the Fermi level,

high-concentration sp^2 carbon clusters in the films play a more important role in determining the electron field emission property of the films. The effect of introducing fluorine into the DLC matrix is to allow an easier formation of sp^2 clusters [35, 36]. From FTIR analysis it was observed that with the increase of fluorine concentration in the DLC films, the sp^2-bonded carbon content in the films increased. In the case of our deposited F:DLC films, the sp^2 regions within the insulating sp^3 matrix are assumed to form conductive channels that extend through the whole thickness of the film to the vacuum. An electron traversing through the channels experiences a high electric field. The effective barrier height is reduced with the addition of fluorine impurity in the DLC matrix.

With increasing fluorine percentage the DLC film changes to a polymer-like film, the optical gap decreases and the sp^2 cluster size increases [8]. From the AFM images we conclude that the grain size as well as the RMS roughness of the F:DLC films increases with increase of F atomic percentage in the films. The DLC films deposited for different atomic percentage of F will consist of an sp^3 matrix with varying sp^2 cluster concentration and size. Therefore, we assumed that lowering of the threshold field with incorporation of F to an increase in the sp^2 bonds and cluster size.

For temperature-dependent field emission, the total current density ($J = J_E + J_T$, where J_E and J_T are the field current and thermionic current density respectively) are given by the simplified FN equation and Richardson equation as [37, 38]

$$J = J_E + J_T \tag{4}$$

$$J = a\phi^{-1}(\beta E)^2 \exp\left(\frac{-sb\phi^{3/2}}{\beta E}\right)\left[\frac{\theta}{\sin(\theta)}\right] + ADT^2 e^{-\phi/KT} \tag{5}$$

where A is a constant about 120 A cm^{-2} K^{-2}, D is the average transmission coefficient of the emitter surface, T is the temperature in kelvin, ϕ is the work function of F:DLC, k is the Boltzmann constant and θ is the temperature correction factor, given by

$$\theta \approx \frac{2.2\pi(kT/q)\phi^{1/2}}{1.959E}. \tag{6}$$

For F:DLC with a work function ~4.7 eV [15] and temperature below 1000 K, the value of $[\theta/(\sin(\theta))]$ in equation (5) is always 1.0, and in our studied temperature range (<350 °C) the highest contribution of thermionic emission is much smaller than the field emission current density, i.e., the measured emission property is dominated by the field emission current because, below 1000 K, the thermionic emission effect is less significant than the field emission effect [39]. Hence equation (5) is reduced to equation (3). Figure 10(a) shows the emission current density (J) versus macroscopic field (E) curves for 15.3 at.% F-doped DLC films for different temperature for an anode–sample separation (d) of 120 μm, and the corresponding FN plot is shown in figure 10(b). It has been observed that the J–E curve in the present work is closely fitted with a straight line. This suggests that the electrons are emitted by a cold field emission process. The threshold fields were in the range 2.2–4.2 V μm^{-1} for the range of temperature. From figure 11 it is clear that, with the increase of temperature, the threshold field decreases and the current density increases. The emission current density strongly depends on the work function. The work function of materials is temperature dependent. Therefore, the decrease of threshold field with the increase of temperature may be due to the decrease of the work function of F:DLC films.

According to the FN plot (figure 10(b)), the slope m (given by equation (7)) would represent the combined effect of the work function and the enhancement of the local electric field, and is given by

$$m = -\frac{b\phi^{3/2}}{\beta}. \tag{7}$$

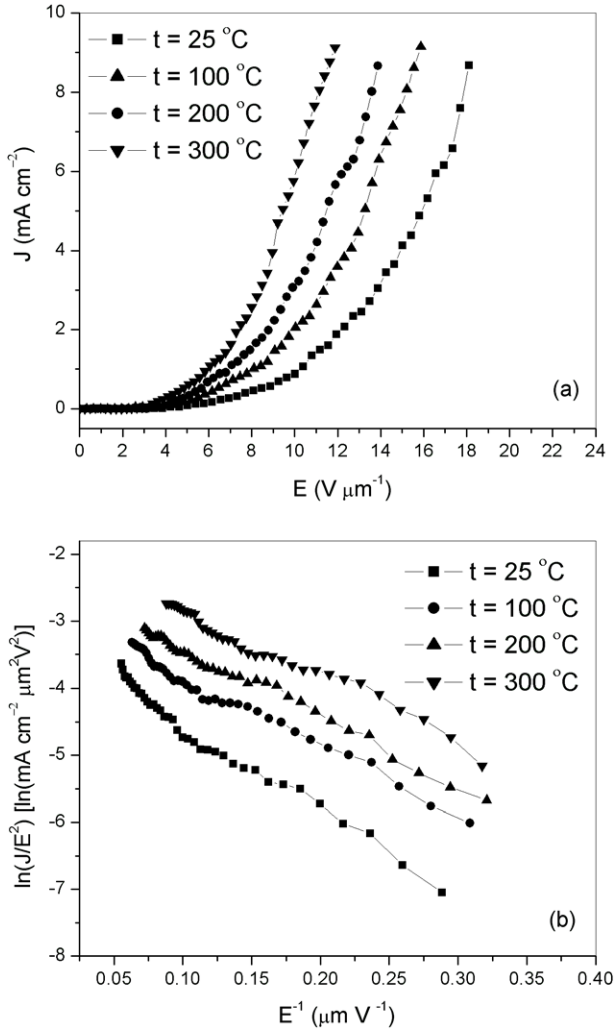

Figure 10. (a) J–E curves of F:DLC (15.3 at.% F) films for different temperature and (b) corresponding FN plot of F:DLC film.

Using $\phi = 4.7$ eV as the work function of F:DLC [14], the field enhancement factor was calculated from the slope of the FN plot; it lies in the range 2784–7411 for the films with different ambient temperature. The field enhancement factor β increases monotonically with the temperature, which explains very well the increase in emission current density with measuring temperature (shown in figure 11). A probable explanation for such a phenomenon is that the presence of a defect band that raises the Fermi level toward the conduction band, and reduces the work function for enhancing field emission. Robertson *et al* [40] suggest that the width of the optical gap is dependent on the cluster size of sp^2 bonding. From defect bands within the band gap, the number of electrons in the conduction band is significantly increased due to electrons transmitting from defect bands. As the temperature increases, the sp^2 bonding, density of the defects, and the conductivity of the DLC film increase [41], so a lower threshold field and higher current density at the same field (shown in figure 11) are obtained.

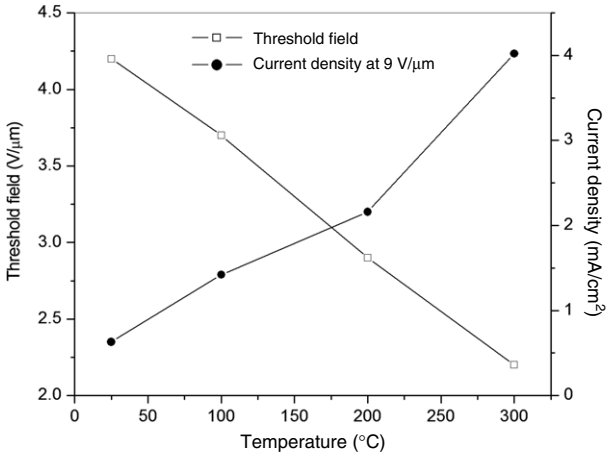

Figure 11. The variation of threshold field and emission current density with temperature for F:DLC (15.3 at.% F) film.

4. Conclusion

Fluorinated DLC in thin film form has been successfully synthesized on glass and silicon substrates via PECVD. The atomic percentage of fluorine in the films has been varied from 0% to 15.3% as measured from energy-dispersive x-ray analysis (EDX). The XPS survey scan of the F:DLC films show clearly the contributions from C 1s (∼285 eV), F 1s (∼687 eV) and O 1s (∼ 532 eV). Fluorine-doped DLC film showed good electron field emission properties with a low threshold field. The threshold field was in the range 2.9–8.5 V μm^{-1} for films with different fluorine concentration and for an anode–sample separation (d) of 100 μm. The temperature-dependent field emission studies of the F:DLC films showed that the threshold field was in the range 4.2–2.2 V μm^{-1} for variation of ambient temperature from 25 to 300 °C. The field enhancement factor was in the range 2784–7411 for the 15.3 at.% F:DLC films with different ambient temperature. The enhancement in field emission properties was attributed to the alteration of the electronic structure by the incorporation of substitutional defect states and the donor activity of fluorine. This study shows that F:DLC films might become good candidates for low-threshold field emitters, among other applications.

Acknowledgment

The authors wish to acknowledge the financial support by the University Grants Commission (UGC), Government of India, under the University with Potential for Excellence Scheme during the execution of the work.

References

[1] Grill A 1999 *Diamond Relat. Mater.* **8** 428
[2] Lifshitz Y 1999 *Diamond Relat. Mater.* **8** 1659
[3] Gabler J, Schafer L and Westermann H 2000 *Diamond Relat. Mater.* **9** 921
[4] Dearnaley G and Arps J H 2005 *Surf. Coat. Technol.* **200** 2518
[5] Endo K and Tatsumi T 1995 *J. Appl. Phys.* **78** 1370
[6] Robertson J 2002 *Mater. Sci. Eng.* R **37** 129

[7] Yokomichi H and Masuda A 2000 *Vacuum* **59** 771
[8] Ronning C, Buttner M, Vetter U, Feldermann H, Wondratschek O, Hofsass H, Brunner W, Au F C K, Li Q and Lee S T 2001 *J. Appl. Phys.* **90** 4237
[9] Ahmed Sk F, Das S, Mitra M K and Chattopadhyay K K 2006 *Indian J. Pure Appl. Phys.* **44** 700
[10] Robertson J 1997 *Thin Solid Films* **296** 61
[11] Tsai C L, Chen C F and Lin C L 2001 *J. Appl. Phys.* **90** 4847
[12] Amratunga G A J and Silva S R P 1996 *Appl. Phys. Lett.* **68** 2529
[13] Ahmed Sk F, Mitra M K and Chattopadhyay K K 2007 *Appl. Surf. Sci.* **253** 5480
[14] Lai S H, Chang K L, Shih H C, Huang K P and Lin P 2004 *Appl. Phys. Lett.* **85** 6248
[15] Tan C M, Jia J and Yu W 2005 *Appl. Phys. Lett.* **86** 263104
[16] Banerjee A N and Chattopadhyay K K 2004 *Appl. Surf. Sci.* **225** 243
[17] Bottani C E, Lamperti A, Nobili L and Ossi P M 2003 *Thin Solid Films* **433** 149
[18] Ronning C, Buttner M, Vetter U, Feldermann H, Wondratschek O, Hofsass H, Brunner W, Au F C K, Li Q and Lee S T 2001 *J. Appl. Phys.* **90** 4237
[19] Yu G Q, Tay B K, Sun Z and Pan L K 2003 *Appl. Surf. Sci.* **219** 228
[20] Liu S, Gangopadhyay S, Sreenivas G, Ang S S and Naseem H A 1997 *J. Appl. Phys.* **82** 4508
[21] Jiang M and Ning Z 2006 *Surf. Coat. Technol.* **200** 3682
[22] Agraharam S, Hess D W, Kohl P A and Allen S A B 1999 *J. Vac. Sci. Technol.* A **17** 3265
[23] Murphy E L and Good R H Jr 1956 *Phys. Rev.* **102** 1464
[24] Forbes R G 1999 *Ultramicroscopy* **79** 11
[25] Gupta S, Weiss B L, Weiner B R and Morell G 2001 *J. Appl. Phys.* **89** 5671
[26] Cao A Y, Zhang X F, Xiao X, Ding M Q, Zhuang D M, Xu C L, Wei B Q, Liang J and Wu D H 2001 *Mater. Lett.* **51** 371
[27] Zhou X T, Lai H L, Peng H Y, Au F C K, Liao L S, Wang N, Bello I, Lee C S and Lee S T 2000 *Chem. Phys. Lett.* **318** 58
[28] Au F C K, Wong K W, Tang Y H, Zhang Y F, Bello I and Lee S T 1999 *Appl. Phys. Lett.* **75** 1700
[29] Okano K, Koizumi S, Silva S R P and Amartunga G A J 1996 *Nature* **381** 140
[30] Silva S R P and Carey J D 2003 *Diamond Relat. Mater.* **12** 151
[31] Ilie A, Ferrari A C, Yagi T and Robertson J 2000 *Appl. Phys. Lett.* **76** 2627
[32] Carey J D, Forrest R D, Khan R U A and Silva S R P 2000 *Appl. Phys. Lett.* **77** 2006
[33] Carey J D, Forrest R D and Silva S R P 2001 *Appl. Phys. Lett.* **78** 2339
[34] Groning O, Kuttel O M, Groning P and Schlapbach L 1997 *Appl. Surf. Sci.* **111** 135
[35] Ishihara M, Suzuki M, Watanabe T, Nakamura T, Tanaka A and Koga Y 2005 *Diamond Relat. Mater.* **14** 989
[36] Valentini L, Braca E, Kenny J M, Lozzi L and Santucci S 2001 *J. Non-Cryst. Solids* **291** 153
[37] Zhu W 2001 *Vacuum Microelectronics* (New York: Wiley) chapter 3
[38] Modinos A 1984 *Field, Thermionic and Secondary Electron Emission Spectroscopy* (New York: Plenum) pp 1–167
[39] Kan M C, Huang J L, Sung J C, Chen K H and Yau B S 2003 *Carbon* **41** 2839
[40] Robertson J and Oreilly E P 1987 *Phys. Rev.* B **35** 2946
[41] Guo P S, Sun Z, Huang S M and Sun Y 2005 *J. Appl. Phys.* **98** 74906